# Bayesian inference of cell-to-cell interactions in low-nutrient neuroblastoma cell cultures

Sara Hamis[1⊙], Khrystyna Hafiichuk[2], Jenny Karlsson[2], David Gisselsson[2], Subhayan Chattopadhyay[2].

**1** Department of Information Technology, Uppsala University, Uppsala, Sweden.
**2** Division of Clinical Genetics, Department of Laboratory Medicine, Lund University, Lund, Sweden.

**Author ORCiDs**: **SH:** 0000-0002-1105-8078, **JK:** 0000-0001-7681-0059, **DG:** 0000-0002-0301-426X, **SC:** 0000-0002-8599-2971.

⊛ **Corresponding author**: sara.hamis@it.uu.se.

**Keywords**: Mathematical model, neuroblastoma, growth characteristics, phenotype switch.

## Abstract

Neuroblastoma is characterised by significant intratumoural heterogeneity which complicates treatments. Phenotypic adaptation, i.e., the ability of cells to alter their phenotype without genetic mutations, is a key factor contributing to this heterogeneity. In this study, we quantify cell actions and cell-to-cell interactions that lead to phenotypic adaptation in vitro under stress. We first record dynamic cell counts in low-nutrient conditions for two cell lines: IMR-32 and SK-N-BE(2). We next formulate a list of permissible biological processes that might occur in the regarded systems and, from the list, construct candidate models via mass action kinetics. To quantitatively infer processes that lead to phenotypic adaptation, we perform a model selection based on computational Bayesian inference methods using the probabilistic programming language Stan. Our results suggest that cell-to-cell interactions promote phenotypic adaptation and that the rate of phenotypic adaptation increases with decreasing nutrient concentrations. We then perform flowcytometry assays to confirm the change in phenotype in the two models and show that the switch occurs as a function of initial condition.

## Introduction

Neuroblastoma (NB), a malignant tumor originating from the sympathetic nervous system, is a leading cause of pediatric cancer mortality (1). Although it is one of the success stories in pediatric oncology, it still exhibits a wide spectrum of clinical outcomes, ranging mostly from clinically responsive to aggressive, high-risk therapy-resistant metastatic disease and rarely spontaneous regression. Often resulting in poor prognosis, global treatment resistance is accepted to be the primary force behind most NB related death. While pangenetic mutations, particularly dysregulating the Ras/MAPK signaling pathway has been shown to be associated therapeutic resistance, emerging evidence suggests that phenotypic plasticity plays a crucial role in enabling NB niche to adapt to environmental stressors. NB cell lines are shown to present with three morphologically distinct phenotypes capable of interconversion: neuroblastic (N), substrate-adherent (S), and intermediate (I) type cells [10]. N-type cells exhibit morphologies of noradrenergic neurons resembling neuroblasts and are characterized by small, round cell bodies with high nuclear-to-cytoplasmic ratios and lower substrate adherence [11]. S-type cells, conversely, resemble epithelial cells or fibroblasts and are flat and large, with an oval nucleus and a large cytoplasm that renders the cells strongly substrate-adherent. The I-type cells possess the capacity to differentiate into N-type and S-type cells. Recently, based on epigenetic profiling of promoter-enhancer interaction and classification of single-cell RNA sequencing, researchers have identified two distinct NB cell states that drive temporary adaptation in response to stimuli and are reminiscent of the N- and S-type differentiation states (adrenergic state: ADRN; mesenchymal state: MES) that also diverge in growth characteristics. While ADRN cells demonstrates accelerated proliferative properties and exhibits increased responsiveness to conventional chemotherapies, MES cells exhibits a dedifferentiated primitive scencent like phenotype that is resistant to treatments.

While the majority of high-risk neuroblastoma tumors initially exhibit an ADRN phenotype making them vulnerable to targeted treatment such as anti-GD2 antibody therapy, a portion of tumors present with mesenchymal predominance. Furthermore, investigation into the nature of the two states show that some NB cells are able to switch between these states based on the tumor environment, a process referred to as phenotypic plasticity. The fluid interaction between ADRN and MES states is very likely responsible for the emergence of treatment resistance in neuroblastoma. This phenotypic plasticity of

ADRN and MES states, results in temporal variations in their admixture in response to dynamic stress conditions. The variation in admixture subsequently influences the population growth characteristics of the NB cells. We hypothesize that by observing these growth characteristics in wild type neuroblastoma model systems of varied phenotypic makeup, it is possible to estimate the relative proportions of cells in the two states, provided that the state conversion rates are realistically accounted for. Previous studies have demonstrated that estimating the relative proportions of two codependently interacting phenotypes within a closed system, based on growth dynamics, can reveal treatment resistance patterns in insulinomas in vitro. Our research aims to extend beyond the point estimates from a snapshot to uncover the underlying mechanistic rules governing phenotypic plasticity in NB in vitro model system. By doing so, we seek to theoretically predict the growth characteristics of a system based on initial observations under a given stress condition (treatment).

**Cell-cell interactions promote phenotypic adaptation in low-nutrient cultures**

To quantify cell actions and cell-to-cell interactions in NB cell cultures under stress, we first in nutrient-poor environments, perform cell count assays of two cell lines, SK-N-BE(2)C and IMR-32, with progressively lowered concentrations of fetal bovine serum (FBS) in the growth media. Counts of the viable cells over up to 20 days in both cell lines

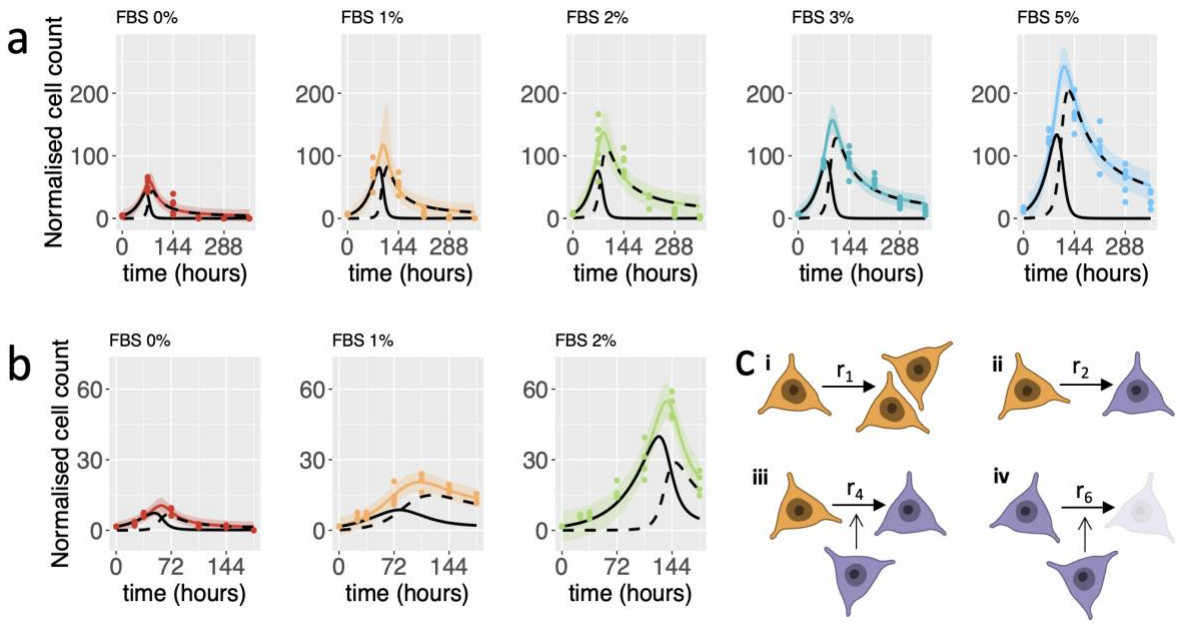


**Fig. 1** In vitro cell counts (dots) and model predictions (means and 90% credible intervals in colored lines and bands) are shown for (a) IMR-32 and (b) SK-N-BE(2) cells. Solid and dashed black lines show q1 and q2 counts, respectively. (c) The inferred processes relate to cell division (i), phenotype switch (ii, iii) and cell death (iv) for q1 (orange) and q2 (purple) cells.

demonstrate non-monotonic growth curves in which cell counts initially increase during a growth phase, reach a peak and subsequently decrease (Figure 1). For the BE cells both peak heights and peak time occurrences increased with increasing FBS concentrations whereas the IMR-32 cells only ever observe a temporally fixed peak of varying counts with a dose response to the FBS concentration.

As a first step towards inferring which underlying cell actions and cell- cell interactions may give rise to this macroscopic cell population behavior, we formulate a list of permissible biological processes that might occur in the cell cultures (Table 1; see Methods for details). As a surrogate to the two-phenotype convention we categorize cells of arbitrary proportions in two abstract phenotype states: state-1 or state-2. Respectively, these describe a more and a less proliferative state and could hypothetically be likened to either N-/S-type cell convention or the recent ADRN/MES superenhancer states. From the list of permissible processes, we construct candidate models such that each candidate model comprises at least one permissible process related either to cell division, phenotypic adaptation, or cell death. Using mass action kinetics, each permissible process is reformulated as a set of ordinary differential equations (ODEs) and, accordingly, each candidate model is described by a system of ODEs in which each term on the right-hand-side corresponds to a permissible process.

All candidate models are evaluated on their ability to fit cell count data and predict unseen data through held-out evaluation (Supplementary Material). A model selection based on held-out evaluation and biological theory reveals that the models that are best able to recapture the observed in vitro dynamics include two common biological processes: state-2 induced state-1-to-2 phenotype switch, and state-2 induced state-2 death.

**Decreasing nutrient concentration increases cell plasticity**

To quantify how the rates of the biological processes in the selected model (model 4) depend on nutrient concentrations, we further analyzed the inferred model parameters. This analysis does not show a linear positive correlation between the rate for spontaneous cell division and FBS concentrations between 0 and 5%, but does show that the cell death rate, promoted by cell- cell interactions, increases with decreasing FBS concentrations. Similarly, the rate of phenotype switch induced by cell-cell interactions increases with decreasing nutrient concentrations. Interestingly, the mode of the rate for

spontaneous phenotype switch remains unchanged while the range increases with increasing FBS concentrations.

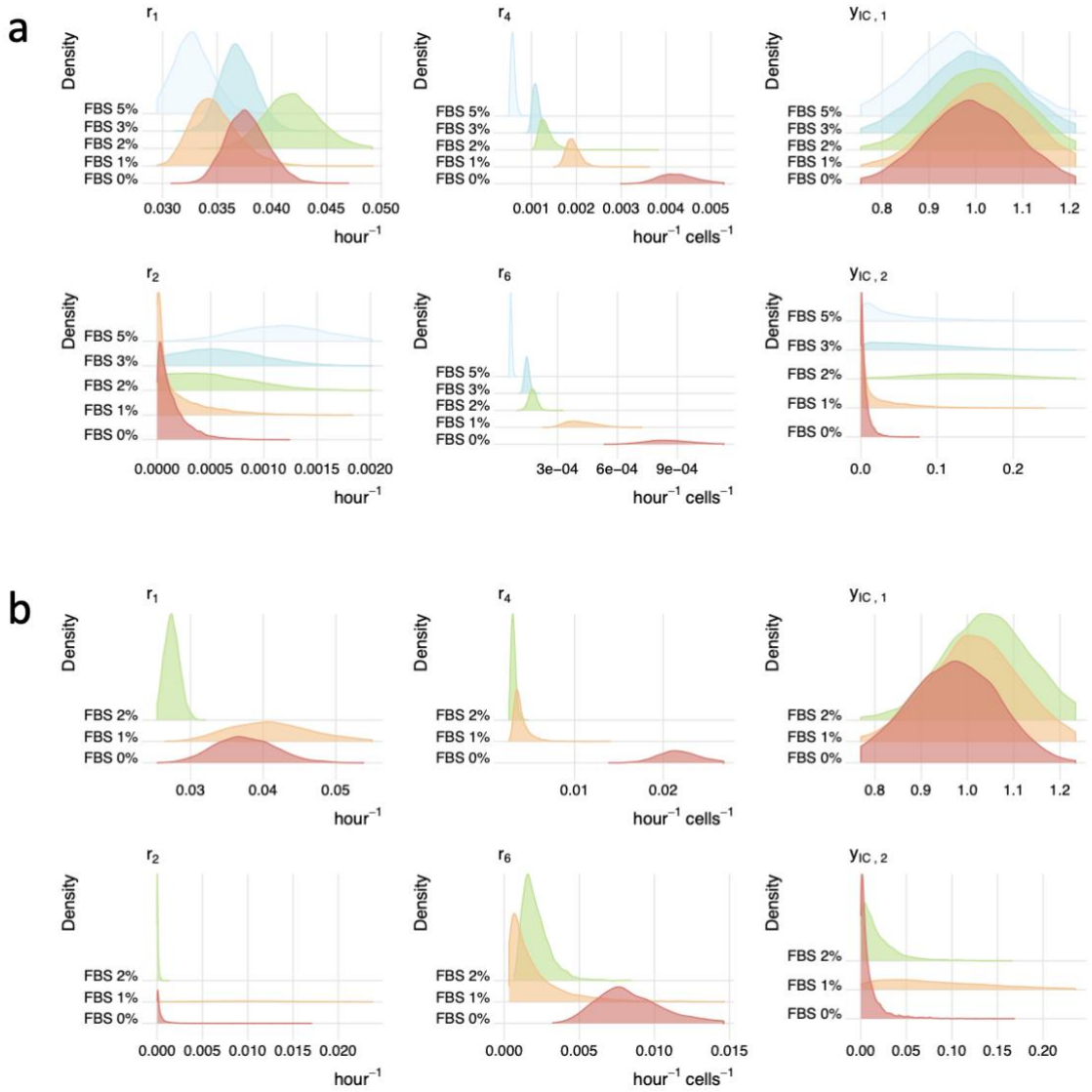


**Fig. 2** Bayesian inference suggests that the rate of phenotypic adaptation increases with decreasing nutrient concentrations. Posterior densities are shown.

## Starting conditions dictate phenotype make up under stress

To further assess the effect of environmental stress on NB cells we performed chemotherapy treatment assays with progressive evaluation of phenotype makeup. We treated IMR cells with 5uM cisplatin for 72 hours and measures surface expression of CD44 and GD2 antibodies. In concordance with what has been shown that under the same treatment conditions BE cells transition from a mixed phenotype to a more MES phenotype, we observed IMR cells making the same transition despite a higher treatment

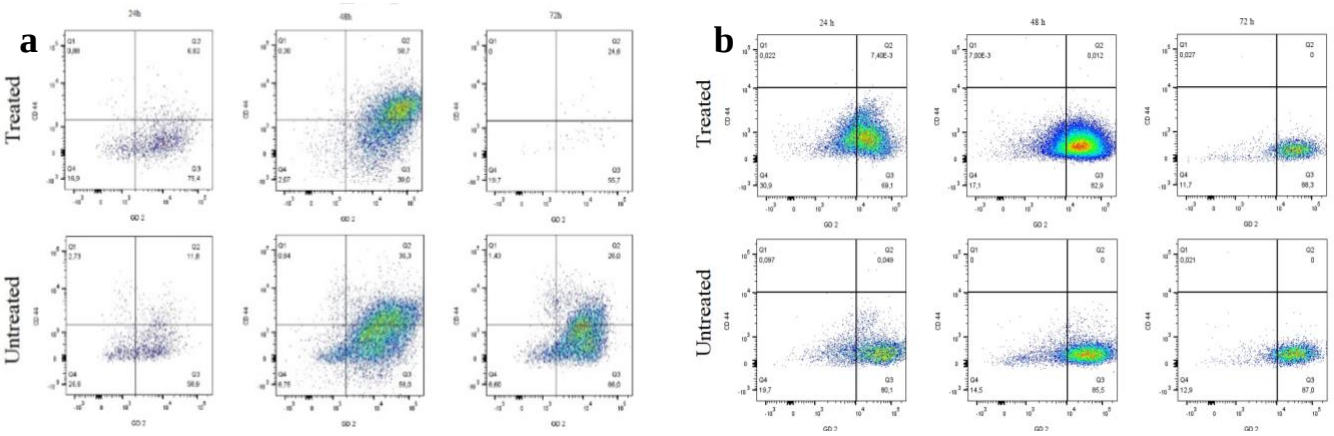


**Fig. 3** Environmental stressor effect on IMR32 cultures. **A**. 5uM Cisplatin treatment over 72 hrs in treated and untreated groups show relative cell populations in Q1 ($CD44^{high}GD2^{low}$), Q2 ($CD44^{high}GD2^{high}$), Q3 ($CD44^{low}GD2^{high}$) and Q4 ($CD44^{low}GD2^{low}$). **B**. Cells in treatment group are cultured in 2% FBS media for 72 hrs and surface expression of CD44 and GD2 are evaluated in a similar manner to that in **A**. Both untreated groups are cell cultured in optimal growth conditions.

response due to its predominantly adrenergic makeup (Figure 3). Within 48hrs of treatment, median CD44 expression increased more than 5e03 folds with a significant difference from the untreated culture ($P < 0.05$, in pooled triplicate cultures) indicating upsurge in mesenchymal phenotype. While the phenotype makeup of the untreated cells remain unchanged over 72hrs, most cells had undergone apoptosis by the end of the assay in the treatment group. We then hypothesized that such changes may not be only treatment driven, but a more general effect of stress in the environment. The IMR cells were hence cultured in a nutrient deficit condition (2% FBS) for 72 hrs. Here we again observed a significantly increased CD44 expression in the treatment group ($P < 0.001$, pooled triplicates).

## Discussion

Although the standard of care chemotherapeutic agents and targeted therapies initially achieve complete response in the majority of NB, these treatments frequently become ineffective over time. This phenomenon has necessitated the escalation of treatment regimens especially for high-risk groups to progressively aggressive and highly toxic combination therapies, such as rapid-COJEC, which incorporates five chemotherapeutic agents. The discovery that NB often comprises two distinct phenotypes, one of which may mediate global cross-resistance, has significantly influenced the field's understanding of clinical outcomes and has informed the design and analysis of pre-clinical experiments.

To address this challenge, it is imperative to understand the ecological and evolutionary

dynamics of cellular populations exhibiting ADRN and MES phenotypes, particularly under environmental stressors, which all therapeutic conditions can be considered as surrogates of. Despite the absence of a clear consensus on the classification of these two phenotypes, the terms ADRN and MES are frequently used inter-changeably to describe both cell types and cell states. A critical distinction between these concepts is that cell types are heritable, whereas cell states are not. Recent research by our colleagues has demonstrated that NB cells in vitro are susceptible to phenotype interconversion, with cells reverting to their original state upon removal of the stressor. Understanding these distinctions is essential for elucidating the eco-evolutionary dynamics of neuroblastoma cell populations under therapeutic pressure and provides robust support for our dynamic state change model driven by interaction rules. This study demonstrates that in the two NB cell line model systems, the wild-type composition of ADRN and MES phenotypes differs. Previous investigations focusing on N and S type cells have reported differences in relative abundance of these types in IMR and BE cells REF. Consistent with these previously published data, we demonstrates that wild-type cell populations of the two cell lines comprise markedly different relative proportions of ADRN/MES, as determined by surface marker expression.

As previously observed and documented, the growth characteristics of these two cell lines exhibit significant differences. BE cells are adherent, comprising a heterogeneous population of undifferentiated as well as differentiated phenotypes, with spindle-like cells forming colony-esq structures during proliferation. Their doubling time is approximately 72 hours under optimal growth conditions. In contrast, IMR cells are nominally-adherent, small, differentiated, and possess a faster doubling time of 40 hours. When subjected to nutrient deprivation stress, the growth characteristics of the two cell lines do not change proportional to the ecological parameters. BE cell population peaks are delayed in proportion to added nutrients, suggesting a rescue of cells with ADRN phenotype and a MES to ADRN transition. Conversely, we show that IMR cultures consistently peak at the same time, with population size proportional to the nutrient richness of the media, indicating the relative abundance of the single ADRN cell state.

Furthermore, we demonstrate that under high stress conditions in vitro, Similar to the BE cells REF IMR cells also shift from an ADRN phenotype- dominated composition to a MES phenotype. However, IMR cells are unable to undergo this transition (ADRN to

MES) to initiate an evolutionary rescue due to its lack of MES phenotype in starting condition resulting in cell death proportional to nutrient deficiency. This observation supports the rule incorporated in our modelling that initial conditions for phenotype switching require a viable mixture of both states. A similar phenomenon was observed in the public goods experiment in vitro in an insulinoma model system REF.

The experimental component of this study is confined to in vitro experiments using only two cell lines which we acknowledge needs expansion to elucidate a more generalized conclusion. In addition, as we describe the initial conditions of the ADRN/MES make up affected the results, the inflection point of population rescue is a joint function of the initial condition and environmental stress levels which remain unexplored. To ascertain that culture carrying capacity did not affect the growth characteristics we performed further growth assays in different size flasks with varied numbers of cells seeded varying the population density which did not produce any disagreement. While our findings are consistent with previously published data and shed light on mechanistic relationship of phenotype switch.

## Methods

### Cell cultures

SK-N-BE(2)C cells well cultured in FBS concentrations of 0%, 1% and 2%. For each FBS concentration, the cell viability of four replicate samples were measured at times 0, 24, 36, 72, 108, 144 and 180 hours, and were multiplied by culture volume to obtain cell counts. IMR-32 cells were cultured in FBS concentrations of 0%, 1%, 2%, 3%, 5% and 10%. For each FBS concentration, the cell viability of six replicate samples were measured at times 0, 48, 96, 168, 240, 312, 384 and 456 hours, and were multiplied by culture volume to obtain cell counts. Cell viability was measured using the Countess™ Automated Cell Counter from Invitrogen with trypan blue staining. After each sampling, FBS concentrations were replenished in the cell cultures.

### Formulation of mathematical candidate models

In our model, we abstractly classify cells as being in one of two phenotype states, $q_1$ or $q_2$, where the former state is more aggressive than the latter. These states are loosely related to the classical neuroblastoma N-type and S-type cells, or to the more recently

categorized noradrenergic and mesenchymal cells. As spatial structures are perturbed in the cell cultures after sampling, in the absence of such data we make the simplifying modelling assumption that all cells in culture are equally likely to interact each other. This assumption allows us to formulate permissible biological processes, which might occur in the in vitro cultures, using law of mass action kinetics. As such, each permissible process can be formulated by a set of ordinary differential equations (ODEs). From these, we define a list of candidate models, each defined by a unique set of permissible processes.

Each permissible processes is denoted by an index $p$ (Figure 1), and each candidate model comprises a set of permissible processes. The set $P^i \subset \{1,2,...,N\}$ is unique to each candidate model $i$, and describes which of the $N$ candidate processes $p$= 1,2,...,$N$ are included in the model (here $N$= 6). For each candidate model, the cell culture system is described by the state vector $\bar{q}$= ($q_1$,..,$q_S$), where $S$i s the number of phenotypes (here $S$= 2). Generally, the $ith$ candidate model is thus de- scribed by a system of ODEs

$$\left(\frac{dq_j(t)}{dt}\right)_i = \sum_{p \in P^i} f_j^p(\bar{q}, t, r_p), \tag{1}$$

where $i$= 1,2,...$M$ and $M$ is the number of candidate models (here $M$= 8). From Figure 1 we can, for instance, see that candidate model 4 is described by four candidate processes: cell division ($p$= 1), spontaneous cell state conversion ($p$= 2), $q_2$-induced cell state conversion ($p$= 4) and $q_2$-induced cell death ($p$= 6). Therefore, $P^4$ = {1,2,4,5} and the model equations are

$$\left(\frac{dq_1(t)}{dt}\right)_4 = \sum_{p \in \{1,2,4,6\}} f_1^p(q_1, q_2, t, r_p) = r_1 q_1(t) - r_2 q_1(t) - r_4 q_1(t) q_2(t), \tag{2a}$$

$$\left(\frac{dq_2(t)}{dt}\right)_4 = \sum_{p \in \{1,2,4,6\}} f_2^p(q_1, q_2, t, r_p) = r_2 q_1(t) + r_4 q_1(t) q_2(t) - r_6 (q_2(t))^2. \tag{2b}$$

Note that, in formulating the candidate models, we have taken a minimal-parameter modelling approach, such that we have models that contain exactly one cell division process, unidirectional cell state conversion processes and one cell death process. This is equivalent to assuming that there is one dominating cell division and cell death process, and one main direction of phenotypic adaptation in the constant FBS concentration. Another model simplification is that, in our model, the rate coefficients $r_k$,$k$= 1,...,$p$ may be functions of FBS concentrations. However,

we assume that they are not functions of time, since nutrient (FBS) concentrations are replenished after sampling in the experimental setup, and the cells do not run out of space.

## Implementation and model selection

The measured experimental outputs correspond to the total cell concentration and does not distinguish between cells in state-1 and state-2. Consequently, the candidate models listed in Table 1 are all structurally non-identifiable. Despite this, in order to make progress in uncovering dynamics in the modelled cell system, we heuristically fit all candidate models to the in vitro data using the probabilistic programming framework Stan and RStan (the R interface to Stan) and then per- form leave-one-out cross-validation to compare the models' performances. Information on how to access, run and modify the code files used in this study are available on the public repository https://github.com/SJHamis/neuroblastoma_dynamics

| Process index | Process | Description | Equation terms | Model index | | | | | | | |
|---|---|---|---|---|---|---|---|---|---|---|---|
| | | | | 1 | 2 | 3 | 4 | 5 | 6 | 7 | 8 |
| *Cell division processes* | | | | | | | | | | | |
| 1 | **Spontaneous $q_1$ cell division** | Cells in state $q_1$ spontaneously divide with rate coefficient $r_1$. | $f_1^1 = r_1 q_1(t)$<br>$f_2^1 = 0$ | ✓ | ✓ | ✓ | ✓ | ✓ | ✓ | ✓ | ✓ |
| *Cell state conversion processes* | | | | | | | | | | | |
| 2 | **Spontaneous cell state conversion** | Cells in state $q_1$ spontaneously convert to $q_2$ with rate coefficient $r_2$. | $f_1^2 = -r_2 q_1(t)$<br>$f_2^2 = r_2 q_1(t)$ | ✓ | ✓ | ✓ | ✓ | | | | |
| 3 | **$q_1$-inducedcell state conversion** | Cells in state $q_1$ induce $q_1$-to-$q_2$ conversion with rate coefficient $r_3$. | $f_1^3 = -r_3(q_1(t))^2$<br>$f_2^3 = r_3(q_1(t))^2$ | | | | | ✓ | ✓ | ✓ | ✓ |
| 4 | **$q_2$-inducedcell state conversion** | Cells in state $q_2$ induce $q_1$-to-$q_2$ conversion with rate coefficient $r_4$. | $f_1^4 = -r_4 q_1(t) q_2(t)$<br>$f_2^4 = r_4 q_1(t) q_2(t)$ | | | ✓ | ✓ | | | ✓ | ✓ |
| *Cell death processes* | | | | | | | | | | | |
| 5 | **Spontaneous cell death** | Cells in state $q_2$ are spontaneously removed from with rate coefficient $r_5$. | $f_1^5 = 0$<br>$f_2^5 = -r_5 q_2(t)$ | ✓ | | ✓ | | ✓ | | ✓ | |
| 6 | **$q_2$-inducedcell death** | Cells in state $q_2$ induce removal of $q_2$ cells with rate coefficient $r_6$. | $f_1^6 = 0$<br>$f_2^6 = -r_6(q_2(t))^2$ | | ✓ | | ✓ | | ✓ | | ✓ |

Table 1: **Candidate biological processes and mathematical models.** The table illustrates which candidate processes 1 to 6 are included in candidate models 1 to 8. Included processes are indicated by check marks (✓).

# References


[1] E. Rodriguez-Fos, M. lix, M. Burkert, M. s, J. Toedling, N. Thiessen, et al. “Mutational topography reflects clinical neuroblastoma heterogeneity”, *Cell Genom* 3.10 (Oct. 2023), p. 100402.

[2] K. I. Lundberg, D. Treis, and J. I. Johnsen. “Neuroblastoma Heterogeneity, Plasticity, and Emerging Ther- apies”, *Curr Oncol Rep* 24.8 (Aug. 2022), pp. 1053–1062.

[3] K. Schmelz, J. Toedling, M. Huska, M. C. Cwikla, L. M. Kruetzfeldt, J. Proba, et al. “Spatial and temporal intratumour heterogeneity has potential consequences for single biopsy-based neuroblastoma treatment decisions”, *Nat Commun* 12.1 (Nov. 2021), p. 6804.

[4] M. Gautier, C. Thirant, O. Delattre, and I. Janoueix-Lerosey. “Plasticity in Neuroblastoma Cell Identity Defines a Noradrenergic-to-Mesenchymal Transition (NMT)”, *Cancers (Basel)* 13.12 (June 2021).

[5] X. Yan, C. R. Kennedy, S. B. Tilkens, O. Wiedemeier, H. Guan, J. I. Park, et al. “Cooperative Cross-Talk between Neuroblastoma Subtypes Confers Resistance to Anaplastic Lymphoma Kinase Inhibition”, *Genes Cancer* 2.5 (May 2011), pp. 538–549.

[6] V. Veschi, F. Verona, and C. J. Thiele. “Cancer Stem Cells and Neuroblastoma: Characteristics and Ther- apeutic Targeting Options”, *Front Endocrinol (Lausanne)* 10 (2019), p. 782.

[7] R. A. Ross, J. L. Biedler, and B. A. Spengler. “A role for distinct cell types in determining malignancy in human neuroblastoma cell lines and tumors”, *Cancer Lett* 197.1-2 (July 2003), pp. 35–39.

[8] M. Piacentini, L. Piredda, D. T. Starace, M. Annicchiarico-Petruzzelli, M. Mattei, S. Oliverio, et al. “Dif- ferential growth of N- and S-type human neuroblastoma cells xenografted into scid mice. correlation with apoptosis”, *J Pathol* 180.4 (Dec. 1996), pp. 415–422.

[9] G. Pelizzo, V. Veschi, M. Mantelli, S. Croce, V. Di Benedetto, P. D’Angelo, et al. “Microenvironment in neuroblastoma: isolation and characterization of tumor-derived mesenchymal stromal cells”, *BMC Cancer* 18.1 (Nov. 2018), p. 1176.

[10] G. Begaud-Grimaud, S. Battu, P. Lazcoz, J. S. Castresana, M. O. Jauberteau, and P. J. Cardot. “Study of the phenotypic relationship in the IMR-32 human neuroblastoma cell line by sedimentation field flow fractionation”, *Int J Oncol* 31.4 (Oct. 2007), pp. 883–892.

[11] V. Ciccarone, B. A. Spengler, M. B. Meyers, J. L. Biedler, and R. A. Ross. “Phenotypic diversification in human neuroblastoma cells: expression of distinct neural crest lineages”, *Cancer Res* 49.1 (Jan. 1989), pp. 219–225.

[12] R. A. Ross, B. A. Spengler, C. nech, M. Porubcin, W. J. Rettig, and J. L. Biedler. “Human neuroblastoma I-type cells are malignant neural crest stem cells”, *Cell Growth Differ* 6.4 (Apr. 1995), pp. 449–456.

[13] M. Piacentini, L. Piredda, D. T. Starace, M. Annicchiarico-Petruzzelli, M. Mattei, S. Oliverio, et al. “Dif- ferential growth of N- and S-type human neuroblastoma cells xenografted into scid mice. correlation with apoptosis”, *J Pathol* 180.4 (Dec. 1996), pp. 415–422.

[14] S. Hopkins-Donaldson, J. L. Bodmer, K. B. Bourloud, C. B. Brognara, J. Tschopp, and N. Gross. “Loss of caspase-8 expression in highly malignant human neuroblastoma cells correlates with resistance to tu- mor necrosis factor-related apoptosis-inducing ligand-induced apoptosis”, *Cancer Res* 60.16 (Aug. 2000), pp. 4315–4319.

[15] N. Bell, V. Hann, C. P. Redfern, and T. R. Cheek. “Store-operated Ca(2+) entry in proliferating and retinoic

acid-differentiated N- and S-type neuroblastoma cells", *Biochim Biophys Acta* 1833.3 (Mar. 2013), pp. 643–651.

[16] A. Valent, J. nard, A. M. nuat, J. Silva, A. Duverger, N. Duarte, et al. "Phenotypic and genotypic diversity of human neuroblastoma studied in three IGR cell line models derived from bone marrow metastases", *Cancer Genet Cytogenet* 112.2 (July 1999), pp. 124–129.

[17] J. Li, Y. Wang, L. Li, P. M. Or, C. Wai Wong, T. Liu, et al. "Tumour-derived substrate-adherent cells promote neuroblastoma survival through secreted trophic factors", *Mol Oncol* 15.8 (Aug. 2021), pp. 2011–2025.

[18] M. Zeineldin, A. G. Patel, and M. A. Dyer. "Neuroblastoma: When differentiation goes awry", *Neuron* 110.18 (Sept. 2022), pp. 2916–2928.

[19] C. Thirant, A. Peltier, S. Durand, A. Kramdi, C. Louis-Brennetot, C. ne, et al. "Reversible transitions between noradrenergic and mesenchymal tumor identities define cell plasticity in neuroblastoma", *Nat Com- mun* 14.1 (May 2023), p. 2575.

[20] I.M. Ambros and P.F. Ambros. "Schwann cells in neuroblastoma", *European Journal of Cancer* 31.4 (1995). Genetics, Cellular Biology and Clinical Management of Human Neuroblastoma, pp. 429–434. ISSN: 0959-8049. DOI: https://doi.org/10.1016/0959-8049(95)00051-J. URL: https://www.sciencedirect.com/science/article/pii/095980499500051J.

[21] Robert A. Ross. "Cellular Heterogeneity", *Neuroblastoma*. Ed. by Nai-Kong V. Cheung and Susan L. Cohn. Berlin, Heidelberg: Springer Berlin Heidelberg, 2005, pp. 55–61. ISBN: 978-3-540-26616-7. DOI: 10.1007/3-540-26616-X_6. URL: https://doi.org/10.1007/3-540-26616-X_6.

[22] N. Cohen, D. R. Betts, G. Rechavi, N. Amariglio, and L. Trakhtenbrot. "Clonal expansion and not cell interconversion is the basis for the neuroblast and nonneuronal types of the SK-N-SH neuroblastoma cell line", *Cancer Genet Cytogenet* 143.1 (May 2003), pp. 80–84.

[23] T. van Groningen, J. Koster, L. J. Valentijn, D. A. Zwijnenburg, N. Akogul, N. E. Hasselt, et al. "Neuroblastoma is composed of two super-enhancer-associated differentiation states", *Nat Genet* 49.8 (Aug. 2017), pp. 1261–1266.

[24] M. Ponzoni, T. Bachetti, M. V. Corrias, C. Brignole, F. Pastorino, E. Calarco, et al. "Recent advances in the developmental origin of neuroblastoma: an overview", *J Exp Clin Cancer Res* 41.1 (Mar. 2022), p. 92.

[25] P. Haridas, C. J. Penington, J. A. McGovern, D. L. S. McElwain, and M. J. Simpson. "Quantifying rates of cell migration and cell proliferation in co-culture barrier assays reveals how skin and melanoma cells interact during melanoma spreading and invasion", *J Theor Biol* 423 (June 2017), pp. 13–25. DOI: https://doi.org/10.1016/j.jtbi.2017.04.017.

[26] A. Kaznatcheev, J. Peacock, D. Basanta, A. Marusyk, and J. G. Scott. "Fibroblasts and alectinib switch the evolutionary games played by non-small cell lung cancer", *Nat Ecol Evol* 3.3 (Mar. 2019), pp. 450–456. DOI: https://doi.org/10.1038/s41559-018-0768-z.

[27] P. Gerlee, P. M. Altrock, A. Malik, C. Krona, and S. Nelander. "Autocrine signaling can explain the emergence of Allee effects in cancer cell populations", *PLoS Comput Biol* 18.3 (Mar. 2022), e1009844. DOI: https://doi.org/10.1371/journal.pcbi.1009844.